but its point-source solutions. For structures with plane-parallel interfaces, the Fourier transform with respect to the horizontal coordinates allows obtaining such an explicit integral representation of the Green's function in the form of the inverse Fourier transform path integrals. In the far field, the acoustic waves are described by asymptotic representations obtained from those integrals using residue technique (for GWs) and the stationary phase method (for bulk acoustic waves).

In the case of an isotropic plate, such a Green's function based model has been developed [7] and experimentally validated [8]. The present work is aimed at the extension of that computer model on the anisotropic case and the analysis, on this base, of the effect of anisotropy on the GW dispersion properties, their angular directivity, and the directivity of the scattered (reflected and transmitted) acoustic waves.

2. Mathematical framework

Let us consider a steady-state time-harmonic oscillation $\mathbf{u}(\mathbf{x})e^{-i\omega t}$, $\mathbf{u}=(u_x,u_y,u_z)=(u_1,u_2,u_3)$, $\mathbf{x}=(x,y,z)=(x_1,x_2,x_3)$, of an elastic layer of thickness h immersed in an acoustic fluid (Fig. 1). Most generally, it may be a laminate composite plate fabricated from anisotropic sublayers V_m: $z_{m+1}\le z\le z_m$, $m=1,2,...,M$. The complex displacement amplitude $\mathbf{u}$ obeys the full set of linear elastodynamics equations:

$$C_{ijkl}u_{i,jk}+\rho\omega^2u_i=0,\quad i=1,2,3, \tag{1}$$

where the elastic stiffness tensor C_{ijkl} and the density ρ are piecewise constant functions of the transverse coordinate z. Hereinafter, the time-harmonic factor $e^{-i\omega t}$ is omitted.

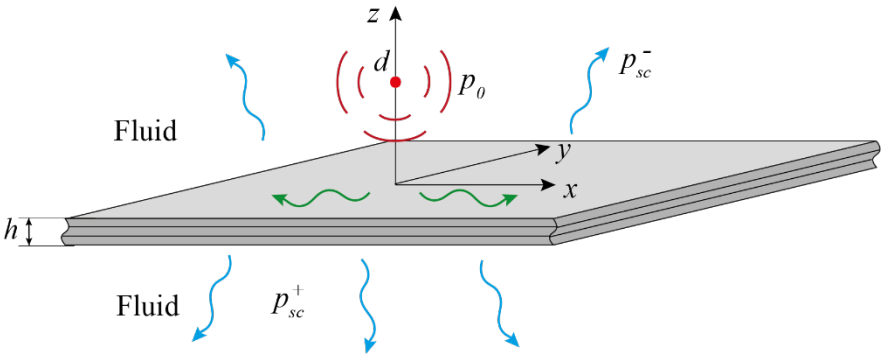

Fig. 1. Geometry of the problem

Acoustic pressure $p(\mathbf{x})$ in the surrounding fluid satisfies the Helmholtz equation:

$$\Delta p+\kappa_0^2p=\delta(\mathbf{x}-\mathbf{x}_0), \tag{2}$$

where $\kappa_0=\omega/c_0$ is a wave number and c_0 is a sonic speed. A monopole source located in the upper half-space at a point $\boldsymbol{x}_0=(0,0,d)$ is modeled by Dirac's delta function; d is the distance from the source to the plate. In the upper half-space $z\ge0$, the total pressure $p(\mathbf{x})$ can be represented as a sum of the direct source field $p_0(\mathbf{x})$ and the reflected field $p_{sc}^-(\mathbf{x})$: $p=p_0+p_{sc}^-$, and in the lower half-space $z\le -h$: $p=p_{sc}^+$, $p_{sc}^+(\mathbf{x})$ is the transmitted field. Here and further, plus and minus are for the acoustic half-spaces $z\le -h$ and $z\ge0$, respectively.

The incident spherical body waves radiated by the monopole source are described by the classical fundamental solution of the Helmholtz equation:

$$p_0 = -\frac{1}{4\pi R} e^{i\kappa_0 R}, R = |\mathbf{x} - \mathbf{x_0}|, \tag{3}$$

while the scattered fields $p_{sc}^{-}(\mathbf{x})$ and $p_{sc}^{+}(\mathbf{x})$ are unknown.

In the fluid, the displacement vector $\mathbf{u}$ is expressed in terms of the pressure p:

$$\mathbf{u} = \frac{1}{\rho_0 \omega^2} \nabla p. \tag{4}$$

The wave fields in the layer and in the fluid are connected by the conditions of continuity of the normal displacements u_z and stresses σ_{zz} at the fluid-solid interfaces:

$$u_z = \frac{1}{\rho_0 \omega^2} \frac{\partial p}{\partial z}, \quad \sigma_{zz} = -p \text{ at } z = 0 \text{ and } z = -h. \tag{5}$$

Here ρ_0 is the density of the acoustic fluid. In addition, these interfaces are free from the tangential stresses:

$$\tau_{xz} = \tau_{yz} = 0 \text{ at } z = 0 \text{ and } z = -h. \tag{6}$$

In the multilayer case, the boundary conditions assume the continuity of displacements $\mathbf{u}$ and stresses $\boldsymbol{\tau} = (\tau_{xz}, \tau_{yz}, \sigma_z)$, i.e. the sublayers are perfectly bonded with each other. These interface boundary conditions are augmented by the radiation conditions at infinity following from the principle of limiting absorption. The displacement and pressure fields in the source-fluid-layer structure are determined via the solution of the boundary value problem (1) - (6) yielding the required Green's function.

The Fourier transform F_{xy} with respect to the horizontal coordinates x and y is applied to Eqs. (1) - (6) with the Fourier parameters α_1 and α_2. This allows obtaining an explicit integral representation of the BVP solution. The unknown fields $p_{sc}^{\pm}$ and $\mathbf{u}$ can be written in terms of their Fourier symbols $P_{sc}^{\pm} = F_{xy}[p_{sc}^{\pm}]$ and $\mathbf{U} = F_{xy}[\mathbf{u}]$:

$$p_{sc}^{\pm}(\mathbf{x}) = F_{xy}^{-1}[P_{sc}^{\pm}] = \frac{1}{4\pi^2} \int_{\Gamma_1} \int_{\Gamma_1} P_{sc}^{\pm}(\alpha_1, \alpha_2, z) e^{-i(\alpha_1 x + \alpha_2 y)} d\alpha_1 d\alpha_2, \tag{7}$$

$$\mathbf{u}(\mathbf{x}) = F_{xy}^{-1}[\mathbf{U}] = \frac{1}{4\pi^2} \int_{\Gamma_1} \int_{\Gamma_1} \boldsymbol{K}_3(\alpha_1, \alpha_2, z) Q(\alpha_1, \alpha_2) e^{-i(\alpha_1 x + \alpha_2 y)} d\alpha_1 d\alpha_2. \tag{8}$$

Here $\boldsymbol{K}_3 = (K_{31}, K_{32}, K_{33})^T$ is the third column of the Green's matrix for the multi-layered half-space $z \le 0$ (an anisotropic laminate plate $-h \le z \le 0$ is underlain by a fluid half-space $z \le -h$) subjected to a surface load q. To calculate the elements of matrix K, we use the stable algorithm for anisotropic laminate composites [9]. Based on the continuity conditions of Eq. (5), the Fourier symbol of the interface load $Q = F_{xy}[q]$ can be explicitly expressed via the Fourier symbol of the source field p_0 at the interface $z = 0$:

$$Q = 2\sigma_0 P_0 / \Delta, \quad P_0 = -\frac{e^{-\sigma_0 d}}{2\sigma_0}, \quad \Delta = \omega^2 \rho_0 K_{33}(\alpha_1, \alpha_2) - \sigma_0, \tag{9}$$

$$\sigma_0 = \sqrt{\alpha^2 - \kappa_0^2}, \ \alpha^2 = \alpha_1^2 + \alpha_2^2, \ \mathrm{Re}\,\sigma_0 \ge 0, \quad \mathrm{Im}\,\sigma_0 \le 0.$$

The Fourier symbols of the reflected and transmitted fields $P_{sc}^{\pm}$ can be written in the forms $P_{sc}^{-} = P^{-} e^{-\sigma_0 (z+d)}$ and $P_{sc}^{+} = P^{+} e^{\sigma_0 (z+h-d)}$, respectively; the constants P^{-} and P^{+}, which control the amplitude of the reflected and transmitted acoustic waves, are expressed via Q and K_{33}: $P^{-} = (\omega^2 \rho_0 + \sigma_0)/(2\sigma_0 \Delta)$, $P^{+} = -\omega^2 \rho_0 K_{33}/(\sigma_0 \Delta)$. The integration paths Γ_1 and Γ_2

go along the real axes rounding the real poles ζ_n of the integrand in accordance with the principle of limiting absorption [10]. These poles are roots of the characteristic (dispersion) equation:

$$\Delta(\alpha_1, \alpha_2, \omega) = 0. \tag{10}$$

3. Bulk and guided waves

Integral representations (7) – (8) provide the exact solution to BVP (1) – (6). These integrals describe the total wave field, i.e., the superposition of all waves of different kinds excited by the point source outside and inside the plate. Individual body and guided waves can be extracted from these path integrals as their far-field asymptotics.

The main contribution to the far-field asymptotics of the reflected and transmitted pressure waves p_{sc}^{-} and p_{sc}^{+} is given by the stationary points $\alpha_{1,0}$, $\alpha_{2,0}$ of the oscillating integrands of Eq. (7) written in the spherical coordinates $(R^{\pm}, \psi, \varphi)$, which are related to the Cartesian coordinates as follows

$$x = R^{\pm}\cos\varphi\sin\psi, \quad y = R^{\pm}\sin\varphi\sin\psi, \quad 0 \le \varphi \le 2\pi,$$

$$z = \begin{cases} R^{+}\cos\psi - h + d, & \pi/2 < \psi \le \pi \quad \text{for} \quad p_{sc}^{+}, \\ R^{-}\cos\psi - d, & 0 \le \psi < \pi/2 \quad \text{for} \quad p_{sc}^{-}. \end{cases}$$

The application of the stationary phase method [10] yields the far-field $p_{sc}^{\pm}$ in the form of spherical acoustic waves [7]:

$$p_{sc}^{\pm}(\mathbf{x}) = a^{\pm}(\varphi,\psi)\frac{e^{i\kappa_0 R^{\pm}}}{R^{\pm}}\left[1 + O\left(\frac{1}{\kappa_0 R^{\pm}}\right)\right], \quad \kappa_0 R^{\pm} \to \infty, \tag{11}$$

$$a^{\pm} = \frac{i\,|\cos\psi|}{2\pi}P^{\pm}(\alpha_{1,0}, \alpha_{2,0})\kappa_0, \quad \alpha_{1,0} = -\kappa_0\cos\varphi\sin\psi, \quad \alpha_{2,0} = -\kappa_0\sin\varphi\sin\psi.$$

The guided waves excited in the plate by the incident field $p_0(\mathbf{x})$ are obtained as the contribution of residues from the poles ζ_n. Being the roots of the integrands' denominator Δ (Eqs. (9) - (10)), these poles coincide with the spectral points (eigenvalues) of the BVP, which are conventionally determined using the modal analysis technique. Therefore, physically, they are wavenumbers of the associated normal modes (eigensolutions), while the residues from these poles, being functions of the transverse coordinate z, coincide up to constant factors with the normal-mode eigenforms. The main advantage of the residues in front of the eigenmodes is that their amplitudes are uniquely determined and one-to-one depends on the source (same as the amplitudes $a^{\pm}(\varphi,\psi)$ in Eq. (10)) while the eigensolutions are source-independent.

In the isotropic case, the problem is axially symmetric, and its solution, and, consequently, the wave characteristics, are independent of the azimuth angle φ. Accordingly, using the cylindrical coordinates:

$$x = r\cos\varphi, \quad \alpha_1 = \alpha\cos\gamma, \quad r = \sqrt{x^2 + y^2},$$
$$y = r\sin\varphi, \quad \alpha_2 = \alpha\sin\gamma, \quad \alpha = \sqrt{\alpha_1^2 + \alpha_2^2},$$
$$z = z, \qquad\qquad 0 \le \gamma, \varphi \le 2\pi,$$

the double integrals of the inverse Fourier transform can be reduced to single path integrals over the contour Γ_+ that goes along the real semiaxis $\mathrm{Re}\,\alpha \le 0,\ \mathrm{Im}\,\alpha = 0$ bypassing the real poles ζ_n in accordance with the principle of limiting absorption [10]. For example, for the

radial and vertical components of the axially symmetric displacement vector $\mathrm{u} = (u_r, u_z)$, Eq. (8) takes the form:

$$u_r(r,z) = \frac{1}{2\pi}\int_{\Gamma_+} S(\alpha,z)Q(\alpha)J_1(\alpha r)\alpha^2 d\alpha,$$
$$u_z(r,z) = \frac{1}{2\pi}\int_{\Gamma_+} R(\alpha,z)Q(\alpha)J_0(\alpha r)\alpha d\alpha. \quad (12)$$

Here S and R are conventional notations for the axisymmetric in the plate (α_1,α_2) components of the third column $\mathbf{K}_3 = (-i\alpha_1 S, -i\alpha_2 S, R)^{\mathrm{T}}$ in the isotropic case [10], J_0 and J_1 are Bessel functions, and Q is specified in Eq. (9) above.

The splitting property $J_m(\alpha r) = \frac{1}{2}[H_m^{(1)}(\alpha r) + H_m^{(2)}(\alpha r)]$ together with the relation between the Hankel functions $H_m^{(2)}(-\alpha r) = (-1)^{m+1} H_m^{(1)}(\alpha r)$ allows expanding the integration path Γ_+ over the supplemented path Γ_- along the negative semiaxis $\mathrm{Re}\,\alpha \le 0$ [9,10]. The resulting integral along the full contour $\Gamma = \Gamma_- \cup \Gamma_+$ can be closed upward in the complex plane α due to the integrands' exponential decrease assured by the Hankel function behavior

$$H_m^{(1)}(\alpha r) = (-i)^m \sqrt{2/(i\pi\alpha r)}\, e^{i\alpha r}[1 + O(|\alpha r|^{-1})], \quad |\alpha r| \to \infty. \quad (13)$$

The residue Cauchy theorem yields asymptotic expansions of such integrals in terms of residues from the poles getting inside the closed contour, i.e. lying above Γ:

$$u_r = \sum_{n=1}^{N} a_{r,n}(z) H_1^{(1)}(\zeta_n r) + O(e^{-\mathrm{Im}\,\zeta_{N+1} r}),$$
$$u_z = \sum_{n=1}^{N} a_{r,n}(z) H_0^{(1)}(\zeta_n r) + O(e^{-\mathrm{Im}\,\zeta_{N+1} r}),\ \zeta_n r \to \infty. \quad (14)$$

Here N is a number of real and closest to the real axis poles ζ_n retained in the truncated series; the poles are numbered in ascending order of imaginary parts: $\mathrm{Im}\,\zeta_{n+1} \ge \mathrm{Im}\,\zeta_n$; the amplitude functions are expressed via residues:

$$a_{r,n} = i\mathrm{res}\, S|_{\alpha=\zeta_n}\, Q(\zeta_n)\zeta_n^2/2,$$
$$a_{z,n} = i\mathrm{res}\, R|_{\alpha=\zeta_n}\, Q(\zeta_n)\zeta_n/2.$$

Due to the exponential behavior of the Hankel functions, specified by Eq. (13), the terms of sums (14) associated with real ζ_n describe cylindrical GWs propagating in the far field ($\zeta_n r >> 1$) with the phase and group velocities $c_n = \omega/\zeta_n$ and $v_n = d\omega/d\zeta_n$ (ζ_n are wavenumbers of these GWs). The terms associated with complex ζ_n are evanescent waves propagating with the phase velocities $c_n = \omega/\mathrm{Re}\,\zeta_n$ and the exponential attenuation, which decrements $\delta_n = 2\pi\,\mathrm{Im}\,\zeta_n/\mathrm{Re}\,\zeta_n$ are controlled by the imaginary parts of these poles.

With a free isotropic elastic layer, the GWs associated with the real poles ζ_n are classical Lamb waves [11]. At any fixed frequency ω, the number of real poles N_r, and, correspondingly, the number of traveling guided waves supported by a layered waveguide, is limited. With increasing frequency, N_r increases because complex poles move toward the real axis, accessing it in turn. The poles' movement in the complex plane α and along the real axis is specified by the complex and real branches of dispersion curves $\alpha = \zeta_n(\omega)$. A typical pattern of the Lamb wave dispersion curves is shown in Fig. 2a. These curves are for a free

steel plate of thickness $h = 6.05$ mm and density $\rho = 8000$ kg/m^3; the velocities of the longitudinal and transverse body waves (*P* and *S* waves) in steel are $c_p = 5780$ m/s and $c_s = 3130$ m/s. Branches associated with antisymmetric and symmetric Lamb waves are conventionally denoted A_0, A_1, A_2... and S_0, S_1, S_2... [12].

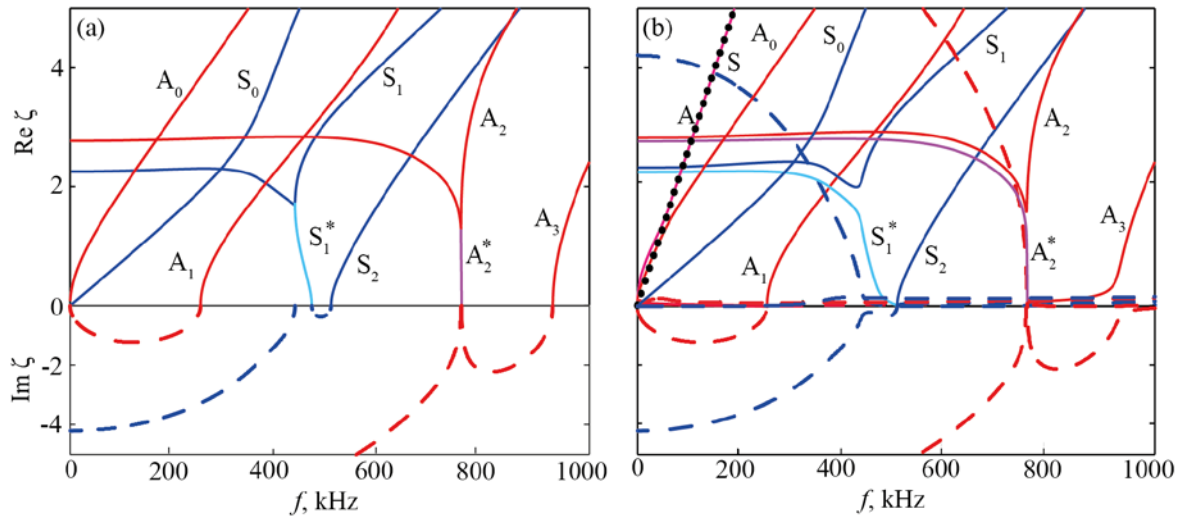

Fig. 2. Dispersion curves for the free (a) and fluid-load (b) steel plate

Under the fluid loading, the real poles shift from the real axis (Fig. 2b), and traveling Lamb waves become leaky Lamb waves [13,14]. They propagate with a weak exponential attenuation induced by relatively small imaginary parts of such former real poles $\mathrm{Im}\,\zeta_n / \mathrm{Re}\,\zeta_n << 1$. In Fig. 2b, the graphs of imaginary parts of such poles go closely to the abscissa axis. The patterns of the real-part curves also changed insignificantly. In addition to leaky Lamb waves, two new guided waves, Scholte-Stoneley waves A and S [15], appear at the fluid-solid interfaces. The roots yielding these waves are pure real (no attenuation). Their curves closely follow the bulk-wave line $\kappa_0 = \omega / c_0$ (Fig. 2b).

4. Influence of anisotropy

While the dispersion curves in Fig. 2 are independent of the direction of propagation specified by the angle φ (same like all other characteristics, including the bulk and guided wave amplitudes $\boldsymbol{a}^{\pm}$ and $\boldsymbol{a}_n^{\pm} = (a_{r,n}, a_{z,n})$), the anisotropy of the immersed composite plate induces such an angular dependence. The numerical examples below demonstrate how the anisotropy affects different waves and wave characteristics. For these examples, we have selected a fiber reinforced composite plate (CFRP) of thickness $h = 2.25$ mm and density $\rho = 1522$ kg/m^3 as a test sample. The fibers are oriented along the *x*-axis, so the composite material is transversally isotropic with the plane of isotropy (*y*, *z*) (Fig. 1). Its elastic properties are specified by the stiffness coefficients [GPa]:

$C_{11} = 121.77,\quad C_{22} = 10.51,\quad C_{33} = 10.51,$

$C_{12} = 3.63,\quad C_{13} = 3.63,\quad C_{23} = 5.29,$

$C_{44} = 2.61,\quad C_{55} = 4.95,\quad C_{66} = 4.95.$

The environment acoustic medium is specified by the density $\rho_0 = 1000$ kg/m^3 and the acoustic velocity $c_0 = 1472$ m/s. The point source is located at the distance *d*=10 mm from the plate.

While in the isotropic case the Fourier symbol K_{33}, and thus the denominator Δ, actually do not depend on the angle γ (axially symmetric in the plane (α_1,α_2)), the anisotropy makes them γ-dependent. Figure 3 illustrates the degree of such dependence of the dispersion curves on γ in a wide frequency range. Along with the change of the curves' patterns, the effect of anisotropy is manifested in the appearance of the pseudo-SH modes, which, in the isotropic case, are polarized strictly horizontally and can, therefore, be excited only by a tangential torsional load.

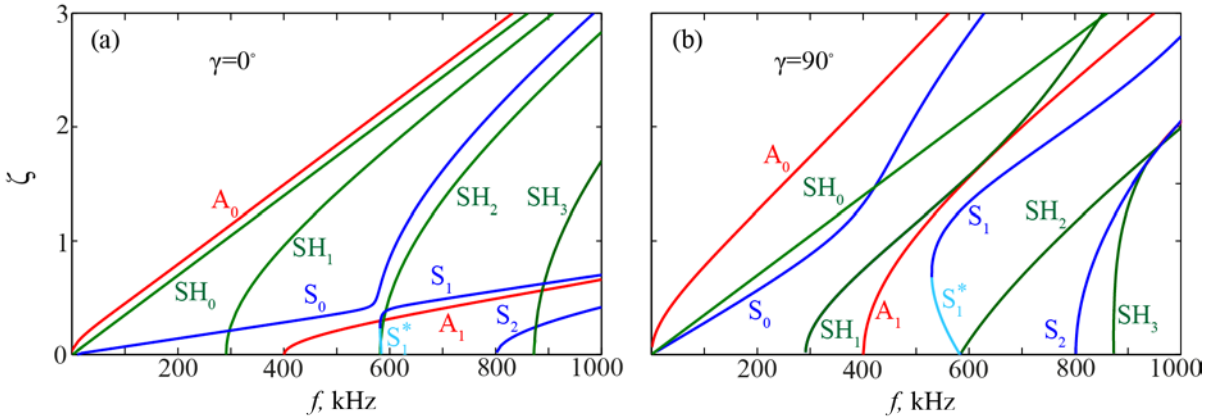

Fig.3. Dispersion curves for the free composite plate in directions $\gamma = 0°$ (a) and $\gamma = 90°$ (b) in the (α,γ) plane

Since the axisymmetry of the Fourier symbols, which were previously axisymmetric in the (α_1,α_2) plane, does not hold, double integrals (7) – (8) cannot be reduced to single integrals over α, but only to repeated integrals over α and γ, and asymptotics (14) cannot be applied. Instead, the GW asymptotics obtained by combining the residue technique with the stationary phase method for the re-integration over γ has been derived [9]. Using this method, the GWs generated by an axisymmetric vertical load $q(r)$ $(Q = Q(\alpha))$ in an anisotropic laminate substrate can be obtained in the following form [16]:

$$\mathbf{u}(\mathbf{x}) = \sum_{n=1}^{N} \mathbf{u}_n(\mathbf{x}) + O((\zeta r)^{-1}),\ \zeta r \to \infty,$$
$$\mathbf{u}_n(\mathbf{x}) = \sum_{m=1}^{M_n} a_{nm}(\varphi, z) e^{is_{nm}(\varphi) r} / \sqrt{\zeta r}, \qquad (15)$$

where ζ is a characteristic wavenumber. Every term $\mathbf{u}_n$ is associated with one generating pole ζ_n, while, generally, it may consist of $M_n > 1$ terms describing cylindrical GWs with the amplitude factors $\boldsymbol{a}_{\mathrm{nm}}$ and the wavenumbers s_{nm}:

$$s_{nm}(\varphi) = s_n(\beta_{nm}),\ s_n(\beta) = \zeta_n(\theta)\sin\beta,\ \theta = \beta + \varphi + \pi/2\,. \qquad (16)$$

The number M_n of wavenumbers is determined by the number of roots β_{nm} of the stationary phase equation:

$$\zeta_n(\theta)\cos\beta + \zeta_n'(\theta)\sin\beta = 0, \qquad (17)$$

where ζ_n' is the derivative of ζ_n with respect to its angular argument. In the special case of isotropic materials, ζ_n are angular independent, hence, $\zeta_n' = 0$, $M_n = 1$, $\beta_{n1} = \pi/2$, and $s_{n1} = \zeta_n$.

The amplitude factors $\boldsymbol{a}_{\rm nm}$ are expressed via the residues of K elements from the poles ζ_n and the values of the Fourier symbol $Q(\alpha,\gamma)$ at the points $\alpha = -s_{nm}$ and $\gamma = \varphi$:

$$\boldsymbol{a}_{nm} = b_{nm}(\varphi, z)Q(-s_{nm}, \varphi), \tag{18}$$

$$b_{nm} = j_n\sqrt{-i\zeta/(2\pi s_n''(\beta_{nm}))}\zeta_n \ \text{res}\ \mathbf{K}_3(\alpha, \theta_{nm}z)|_{\alpha=\zeta_n}.$$

The coefficient j_n is nearly always $j_n = 1$, except in the case of infrequent irregular real poles yielding backward modes for which $j_n = -1$.

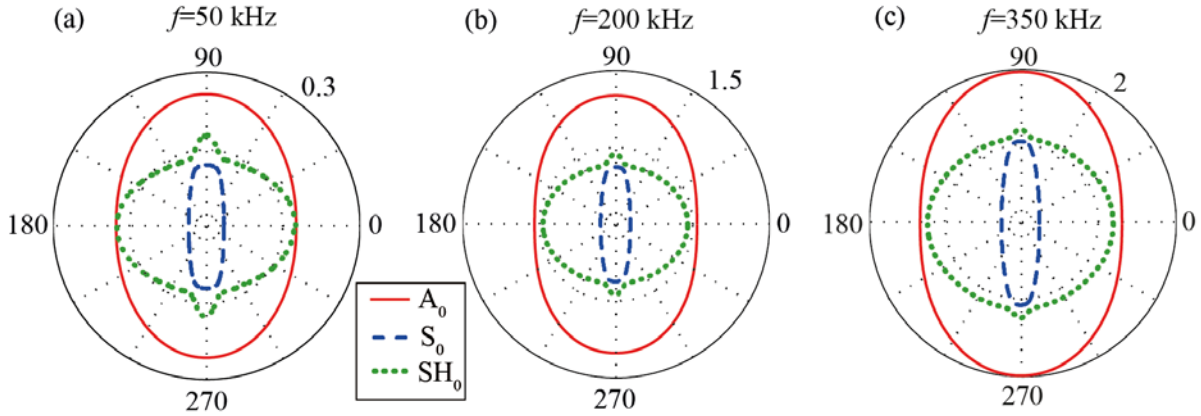

Fig. 4. Angular diagrams for the wavenumbers of the fundamental Lamb modes in the test composite plate; with the immersed plate, the $\text{Re}\,\zeta_n(\gamma)$ diagrams are practically the same

It can be seen from Fig. 3 that the anisotropy significantly affects the dispersion properties in those two mutually orthogonal principal directions $\gamma = 0°$ and $\gamma = 90°$. To show you more fully the effect of anisotropy on the angular dependence of wave characteristics, we have selected three trial frequencies: f = 50, 200 and 350 kHz. Then we computed angular diagrams for the poles ζ_n, amplitudes $\boldsymbol{a}_n$ and attenuation factors $\text{Im}\,\zeta_n$ of the fundamental Lamb modes A_0, S_0 and SH_0 as well as Scholte-Stoneley waves A, S and scattered acoustic waves p_{sc}^- and p_{sc}^+ generated at these frequencies by a given surface load (Figs. 4 – 8).

The analysis of angular diagrams $\text{Re}\,\zeta_n(\gamma)$ (Fig. 4) shows that the regular circles of the isotropic case are transformed into smooth ellipse-like curves, which shapes are almost independent on frequency. The diagrams of the imaginary parts $\text{Im}\,\zeta_n(\gamma)$, which appear under the fluid loading and specify the attenuation of leaky Lamb waves, are of the more intricate form (Fig. 5). The most striking fact is that, unlike the isotropic case, certain angles may exist (the principal directions $\varphi = 0°$, 90°, 180° and 270° in the case) for which $\text{Re}\,\zeta_n(\gamma) = 0$, i.e., the corresponding leaky waves degenerate into ordinary traveling waves propagating in these directions without exponential decay.

The amplitude diagrams (Fig. 6) are the most intricate and frequency sensitive. Such behavior is a manifestation of the frequency dependent directivity of guided waves excited by an axisymmetric surface load in an anisotropic composite plate. This phenomenon is

discussed in details, and its mechanism is theoretically explained and experimentally confirmed in Ref. [17].

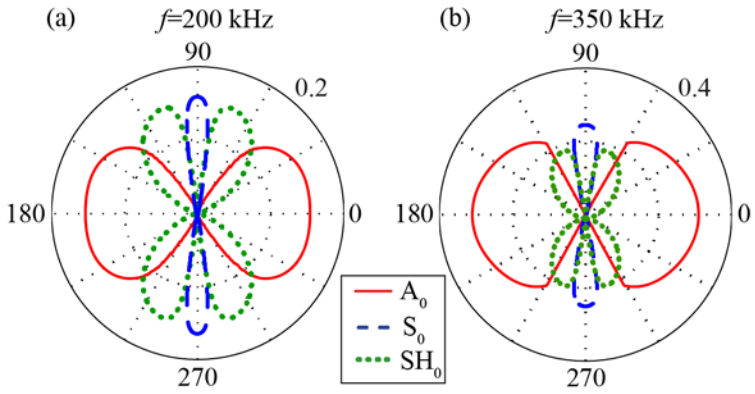

Fig. 5. Angular diagrams for the imaginary parts $\mathrm{Im}\,\zeta_n(\gamma)$ for two trail frequencies; to be well visible, the results for S_0 and SH_0 are multiplied by 10 at f = 200 kHz and by 2 at f = 350 kHz; for f = 50 kHz, $\mathrm{Im}\,\zeta_n = 0$ within the accuracy of 10^{-6}

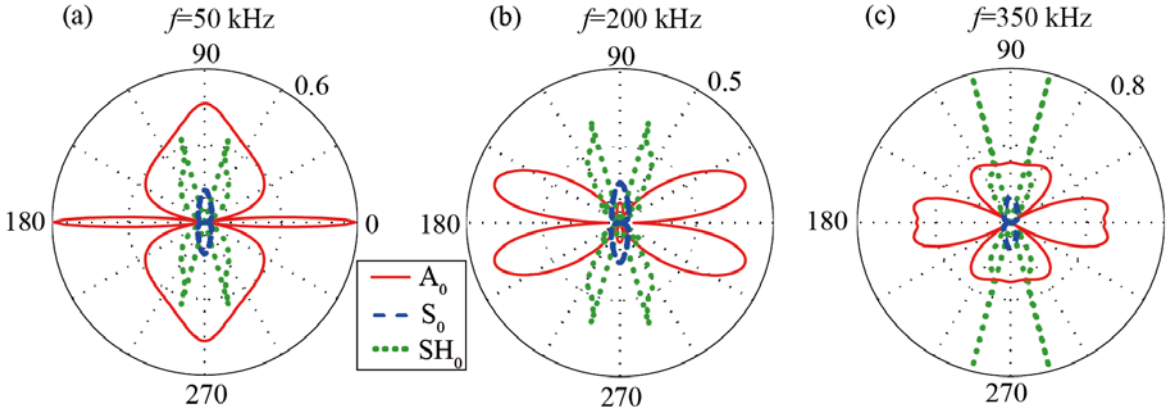

Fig. 6. Angular diagrams for the GW amplitude factors $|\boldsymbol{a}_n(\varphi)|$ related to the surface load (the amplitudes of S_0 and SH_0 waves are multiplied by 100 for (a) and 5 for (b))

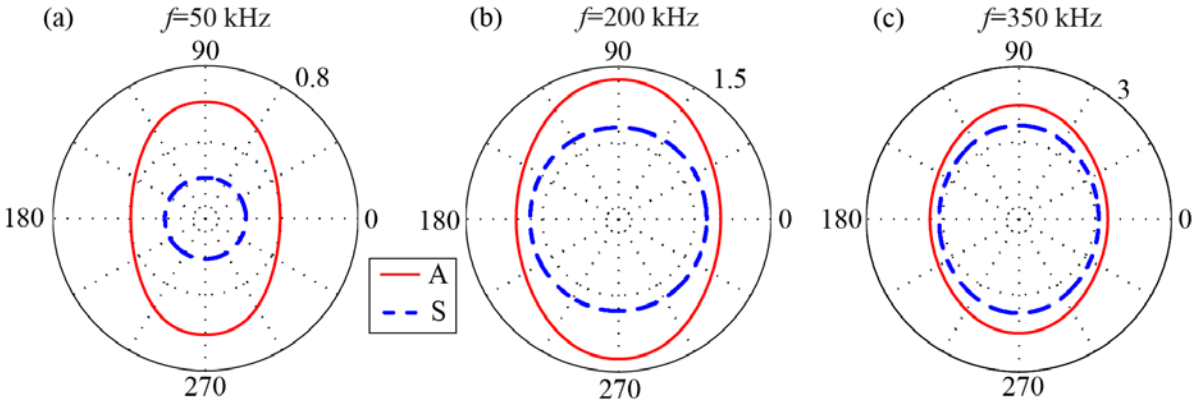

Fig. 7. Angular diagrams $\zeta_n(\gamma)$ for the Scholte-Stoneley modes A and S

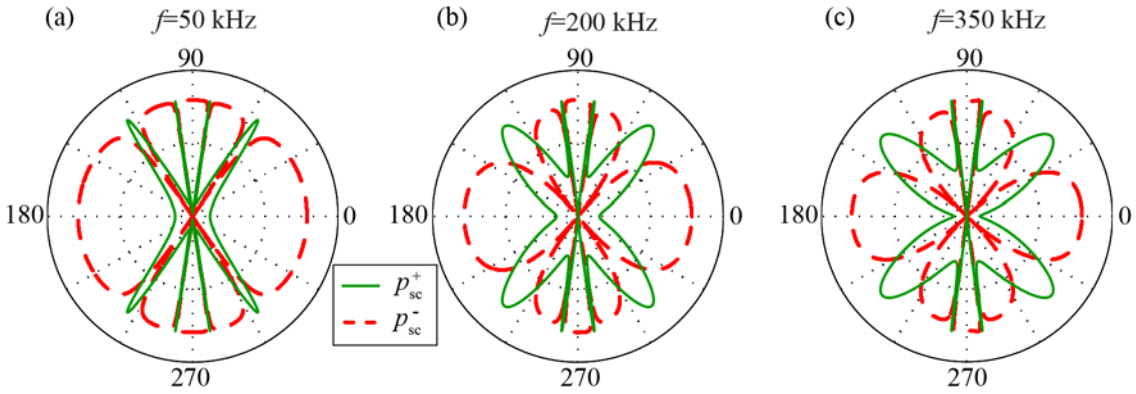

Fig. 8. Angular diagrams of the amplitude factors $|a^{\pm}(\varphi,\psi)|$, $\psi = 45°$, of the transmitted and reflected acoustic waves $p_{sc}^{\pm}$ related to that of the incident pressure p_0

As for the Scholte-Stoneley waves, the diagrams of the A-mode wavenumber become of ellipse-like shape at once, while that of the S-mode remains angular-independent at low frequencies (Fig. 7).

Although the acoustic medium is homogeneous and isotropic, the plate anisotropy also strongly affects the shape of the angular scattering of the reflected and transmitted acoustic waves (Fig. 8). Mathematically, it influences the scattered field through the denominator Δ of form (9) in P^{-} and P^{+}. It depends on γ via $K_{33}(\alpha,\gamma)$. In the case considered, the plate anisotropy results in the reflection which becomes dominant with frequency in the principal directions (Fig. 8c, dashed line), while the maximal transmission occurs in the intermediate directions (solid line).

5. Conclusion

An analytically based computer model for the fluid-loaded anisotropic plate has been developed on the basis of explicit integral and asymptotic representations for the generated and scattered wave fields. On this base, the influence of the fluid loading and plate anisotropy on the dispersion curves, amplitude diagrams, and guided wave attenuation are numerically analyzed and discussed.

Acknowledgement. *The work is supported by the Russian Science Foundation (Project No. 17-11-01191).*

References

[1] Brekhovskikh LM. *Waves in Layered Media*. New York: Academic Press; 1960.

[2] Babich VM, Buldyrev VS. *Asymptotic Methods in Short-Wavelength Diffraction Theory*. Oxford: Alpha Science Intl Ltd; 2009.

[3] Machevariani MM, Tyutekin VV, Shkvarnikov AP. Impedance method for calculating the characteristics of elastic layered inhomogeneous media. *Akusticheskij Zhurnal*. 1971;17(1): 97-102. (In Russian)

[4] Achenbach JD. *Wave Propagation in Elastic Solids*. North Holland: Elsevier; 1973.

[5] Schoenberg M. Plane wave propagation in Stratified anisotropic media. *The Journal of the Acoustical Society of America.* 1974;55(5): 922-924.

[6] Nayfeh AH, Chimenti DE. Propagation of guided waves in fluid-coupled plates of fiber-reinforced composite. *The Journal of the Acoustical Society of America.* 1988;83(5): 1736-1743.

[7] Glushkov EV, Glushkova NV, Miakisheva OA. The interaction of source-generated spherical waves with an elastic plate immersed in acoustic fluid. In: *Proceeding of the International Conference Days on Diffraction 2015 (May 25-29, 2015, St. Petersburg, Russia)*. IEEE; 2015. p.107-111.
[8] Glushkov EV, Glushkova NV, Miakisheva OA. Resonance transmission and backward leaky waves in the coupled system: ultrasound transducer -acoustic fluid - immersed plate. In: *Proceedings of the International Conference Days on Diffraction 2017 (June 19 – 23, 2017, St. Petersburg, Russia).* IEEE; 2017. p.134-140.
[9] Glushkov E, Glushkova N, Eremin A. Forced wave propagation and energy distribution in anisotropic laminate composites. *Journal of the Acoustical Society of America*. 2011;129(5): 2923-2934.
[10] Vorovich I, Babeshko V. *Dynamic Mixed Problems of Elasticity for Nonclassical Domains*. Moscow: Nauka; 1974. (In Russian)
[11] Lamb H. On Waves in an Elastic Plate. *Proceedings of the Royal Society of London*. 1917;93(648): 114-128.
[12] Viktorov IA. *Sound Surface Waves in Solids*. Moscow: Nauka; 1981. (In Russian)
[13] Rokhlin SI, Chimenti DE, Nayfeh AH. On the topology of the complex wave spectrum in a fluid-coupled elastic layer. *Journal of the Acoustical Society of America*. 1989;85(3): 1074-1080.
[14] Simonetti F, Lowe MJS. On the meaning of Lamb mode nonpropagating branches. *Journal of the Acoustical Society of America.* 2005;118(1): 186-192.
[15] Sessarego JP, Sagéloli J, Gazanhes C, Überall H. Two Scholte–Stoneley waves on doubly fluid-loaded plates and shells. *Journal of the Acoustical Society of America*. 1997;101(1): 135-142.
[16] Glushkov E, Glushkova N, Eremin A, Lammering R. Group velocity of cylindrical guided waves in anisotropic laminate composites. *Journal of the Acoustical Society of America*. 2014;135(1): 148-154.
[17] Glushkov E, Glushkova N, Eremin A, Lammering R, Neumann M. Frequency dependent directivity of guided waves excited by circular transducers in anisotropic composite plates. *Journal of the Acoustical Society of America.* 2012;132(2): EL119-EL124.